Article:
Yildizbakan, L., Iqbal, N. orcid.org/0000-0002-2801-707X, Giannoudis, P.V. orcid.org/0000-0002-5205-7696 et al. (1 more author) (2024) Synthesis of Chitosan and Ferric-Ion (Fe^{3+})-Doped Brushite Mineral Cancellous Bone Scaffolds. Biomimetics, 9 (6). 308. ISSN 2313-7673

https://doi.org/10.3390/biomimetics9060308

Synthesis and Engineering of Cancellous Bone Scaffold Derived from Freeze-Dried Ferric-ion (Fe3+)-doped Brushite

By Lemiha YILDIZBAKAN

WORD COUNT 8844
TIME SUBMITTED 08-APR-2024 03:41AM
PAPER ID 108122545

Synthesis and Engineering of Cancellous Bone Scaffold Derived from Freeze-Dried Ferric-ion (Fe^{3+})-doped Brushite

Lemiha Yildizbakan[1*], Neelam Iqbal[1], Peter V. Giannoudis[2], and Animesh Jha[1*]

[1]School of Chemical and Process Engineering, University of Leeds, Leeds, LS2 9JT, UK

[2]Academic Department of Trauma and Orthopaedic Surgery, School of Medicine, University of Leeds, Leeds, LS2 9JT, UK

* Corresponding Authors: (lemiha.yildizbakan1@gmail.com (L.Y.); a.jha@leeds.ac.uk (A.J.))

Abstract

Biodegradable scaffolds are needed for repairing bone defects. To promote the resorption of scaffolds, a large surface area is needed for promoting neo-osteogenesis, which is why in this article, we describe the synthesis and freeze-drying methodologies of ferric-ion (Fe^{3+}) doped brushite, which has been known for favouring the *in situ* condition for osteogenesis.

In this investigation, the role of chitosan during the synthesis of brushite was explored for enhancing the antimicrobial, pore distribution in scaffold volume, and mechanical properties after freeze-drying. During the synthesis of brushite, the calcium nitrate solution was hydrolysed with a predetermined stoichiometric concentration of ammonium phosphate. During the hydrolysis reaction for the formation of brushite ($CaHPO_4.2H_2O$), iron (Fe^{3+}) nitrate ($Fe(NO_3)_3$) was also incorporated, and several Fe^{3+}-ion doped (0-50 weight %), the Dicalcium phosphate (brushite) with were precipitated (Fe^{+3}-DCPD). A range of mixtures of chitosan mixed with Fe^{3+}-DCPD minerals were stir-mixed before the freeze-drying steps. The structural, microstructural, and mechanical properties of freeze-dried materials were characterized.

Keywords: Fe^{+3} –doped brushite (Dicalcium phosphate dihydrate); chitosan; mechanical properties; scaffold; bone tissue engineering

1. Introduction

Bone is a complex living tissue which experiences metabolic and regenerative disruptions when damaged. Impaired bone healing can be caused by insufficient vasculature, infection, limited cell growth, scaffold failure, and may lead to non-union [1]. It has been reported that on average bone tissue regenerates at a rate of around 1 μm per day, making self-repair nearly impossible for severe defects [2]. In addition, for regrowing a damaged bone, the biomechanical stability for the structural continuity of the tissue is essential for the process of regeneration. Bone graft replacement is the most common surgical procedure for filling critical defects (3cm or more) which is necessary to reduce the need for harvesting autografts from patients. Globally, nearly 2 million patients each year need critical defect void-filling procedures [3]. The allografts and xenografts do not offer a better solution than the autograft, because of the increased risk of immune response and infection which may then demand revision surgery [4]. However, autograft harvesting has been linked to increased morbidity at the donor site after surgery [5][6]. Engineering a methodology for fabricating scaffolds that supports osteogenesis and angiogenesis might be able to bridge the gap in the growing demand for biocompatible and resorbable scaffolds [7].

Scaffolds are significant in tissue engineering as they promote and guide new tissue development *in vivo,* performing as a matrix for cell anchoring, inducing particular cellular responses, transporting nutrients and growth factors, and are responsible for cell retention in repairing the defect [8].

An ideal bone scaffold should have biocompatibility, non-toxicity, osteogenic potential to promote new bone growth, load-bearing properties, and a porous structure for nutrient circulation during fracture healing [9]. Natural polymers frequently have highly organised structures that can help cells grow at different phases of development. Crustacean and mushroom-derived chitosan (CS) are widely used biopolymers for various biological purposes, including bone tissue engineering [10]. The chemical structure of chitosan is a linear polysaccharide comprising glucosamine and N-acetyl glucosamine units, connected by β (1-4) glycosidic linkages. Chitosan is a biodegradable polymer with haemostatic characteristics and also has antibacterial activity and biocompatible properties, which are beneficial for bone tissue engineering applications [11]. Chitosan, as a polymeric material, has shown promise for bone regeneration [12,13], particularly when combined with minerals such as calcium phosphate (CaP) ceramics or apatites [14,15]. It is widely known that CaP improves osteoconductivity and scaffold degradation [16,17] and has been reported to stimulate the adhesion, proliferation, and differentiation of bone marrow mesenchymal stem cells [18,19]. The bioactivity of CaPs has been linked to the composition and structure comparable to the mineral phase of bone [20]. Biomaterials utilised in bone implants should have the potential to resorb, giving way to regenerated bone. At pH 7, the thermodynamic solubility of CaP decreases from dicalcium phosphate dihydrate (DCPD)> octacalcium phosphate (OCP) > tricalcium phosphate (TCP) > hydroxyapatite (HAP), proving that the DCPD is the most soluble form amongst the four phosphates [21]. The apparent solubility of DCDP, TCP, and OCP in aqueous media determines the condition for the precipitation of biological apatite precursor for new bone formation and mineralisation [22,23]. The resorption studies on DCPD minerals demonstrate that the mineral exhibits excellent biological characteristics by regulating pH locally by making Ca^{2+}, HPO_4^{2-}, OH^- and H^+ ions available as starting ingredients *in vitro* and in vivo environments for new bone formation [24]. By comparison, it was found that when the porous cylindrical HAP scaffolds were implanted into the cancellous bone of rabbits, after six months, it resorbed slowly (~5.4% in volume) [25]. By contrast, the TCP minerals resorbed far more rapidly (85.% in volume) than HAp under the same pH condition [3,25]. Because of the chemical bonding, the CaPs are inherently brittle and exhibit poor mechanical properties. However, combining CaPs with ions in the lattice, such as silicon (Si^{4+}), zinc (Zn^{2+}), iron (Fe^{2+}/Fe^{3+}), and magnesium (Mg^{2+}) [26–28] is known to reduce brittleness. Doping DCPD with 10mol% of Fe^{2+} and Fe^{3+} ions yielded produced an optimal combination of biomechanical properties for osteogenesis [26].

In this article, we have focussed on using the concept of Fe^{3+}-ion doping of DCPD (Fe^{3+}-DCPD) by mixing with chitosan in a weight proportion of 0 to 50 ratio before freeze-drying for fabricating a highly porous cancellous scaffold. A range of data for the freeze-dried cancellous structure are presented, and these are specified in three different categories: materials structural, mechanical properties, and cell biological characterisations, which are described in detail below.

2. Materials and Methods

2.1 Synthetic Cancellous Bone Scaffolds

A 3 (wt) % chitosan stock solution was prepared to fabricate the synthetic cancellous structure, needed for bone formation. High molecular weight chitosan flakes (Sigma-Aldrich, CAS: 9012-76-4, Taufkirchen, Germany, 3,100,000–3,750,000 Da,>75 % deacetylated) were dissolved in 2 (v/v) % acetic acid (AcrosOrganics, Geel, Belgium, MFCD00036152) solution under continuous mixing for 24hrs for the removal of air bubbles.

Fe^{+3}-DCPD mineral ($Ca_{0.9}Fe_{0.1}HPO_4{\cdot}2H_2O$) was synthesised by a slow dripping to initiate the precipitation process of CaP. 200 ml of distilled water was mixed with 0.1 M of $Ca(NO_3)_2.4H_2O$ (Fisher Chemicals, CAS:13477-34-4, Hampton, VA, USA), and then 20 ml of the prepared solution was mixed with 180 ml of distilled water at 37°C. Following that, 0.83g of iron (Fe^{3+}) nitrate (10 ((mol) %) (VWR Chemicals, CAS:7782-61-8, Leicestershire, UK) was mixed into calcium nitrate solution which was stirred continuously using a magnetic stirrer. This solution we designate as **Solution (A)**. In 200 ml of distilled water, 0.1 M of ammonium phosphate (Acros Organics, CAS: 7783-28-0, Geel, Belgium) was dissolved, and 20 ml of solution was mixed with 180 ml of distilled water, **Solution (B)**. Afterwards, solution (B) was mixed drop-by-drop into solution (A) by continuous mixing for 2 hrs. The mixture of A and B was then left to settle for 1 hour. The Fe^{3+}-DCPD precipitate was filtered using Whatman Grade 44 filter paper (Merck, WHA1444110, Darmstadt, Germany) and washed three times using distilled water. The collected mineral was placed into a furnace and dried for 24 hrs at 80 °C.

Freeze-dried mineral-free and Fe^{3+}-DCPD mineral-loaded chitosan scaffolds: The mineral-free and different concentrations of Fe^{3+}-DCPD mineral (20, 30, 40 and 50 (wt) %) loaded chitosan stock solutions were continuously mixed via a magnetic stirrer for 6 hrs, producing homogenous suspensions. Measured amounts of unloaded and Fe^{3+}-DCPD mineral-loaded CS solutions were frozen at –80 °C for 24 hrs and then transferred into a freeze drier (VirTis 4 KB ZL Benchtop K (SP Industries, Warminster, PA, USA)) machine at -100 °C and pressure of 43 mTorr for 24 hrs.

The freeze-dried samples of mineral-free and Fe^{3+}-DCPD-loaded chitosan scaffolds were treated with 1M sodium hydroxide NaOH (Sigma-Aldrich, CAS: 1310-73-2) for 10 minutes to decrease the CS dissolution rate. After the stipulated duration, the scaffolds were washed 5 times with deionized water to remove the traces of NaOH. The code names of fabricated freeze-dried scaffolds are displayed in Table 1.

Table 1 Summary of the fabricated freeze-dried undoped and Fe^{3+}-DCPD doped chitosan scaffolds with code names.

Code	Description	Fe-DCPD: CH
Fe^{+3}-DCPD	10 (mol) % Iron (III) nitrate doped Dicalcium Phosphate Dihydrate	100 : 0
CH	Chitosan	0: 100
20-Fe^{3+}-DCPD	20 (wt) % Fe-DCPD mineral-loaded chitosan scaffold	20: 80
30-Fe^{3+}-DCPD	30 (wt) % Fe-DCPD mineral-loaded chitosan scaffold	30: 70
40-Fe^{3+}-DCPD	40 (wt) % Fe-DCPD mineral-loaded chitosan scaffold	40: 60
50-Fe^{3+}-DCPD	50 (wt) % Fe-DCPD mineral-loaded chitosan scaffold	50: 50

2.2 Freeze-dried Materials Characterisation Techniques

Renishaw inVia Raman microscope with a laser excitation source at a 785 nm wavelength and 24.9 mW launch power was used, which after focussing via x50 objective lens reduced to <5mW. The incident power of less than 5mW was necessary to prevent photo-damage of the samples during spectroscopic analysis. All freeze-dried samples listed in Table 1 were analysed to ascertain the change in the molecular bonds with the composition of minerals suspended in the chitosan mixture. The frequency of the vibrational range was from 10 cm^{-1} to 3000 cm^{-1}.

The Vertex 70 FTIR spectrometer (Billerica, MA, USA), with the attenuated total reflection (ATR) mode, was used to analyse the fabricated freeze-dried scaffolds by molecular vibration spectroscopy analysis. A mid-IR (MIR) lamp was used as the light source, and the beam splitter was KBr. Every scaffold conducted 32 scans with a spectral resolution of 4 cm^{-1} between 400 cm^{-1} and 4000 cm^{-1}.

Samples were characterised using a D8 X-ray diffractometer with the Cu Kα radiation (λ = 0.15406 nm) in the 5° to 80° Bragg angle (2θ) scanning range with a step size of 0.065 and a scan speed of 0.014° s^{-1}. The Rietveld refinement was used to determine the crystallinity of samples through peak shape and intensity analysis, and HighScore Plus software (PANalytica X'Pert HighScore Plus v3.0, Malvern, UK) was used to evaluate recorded patterns.

The average crystallite size distribution in freeze-dried fabricated scaffolds (CH, 20-Fe^{3+}-DCPD, 30-Fe^{3+}-DCPD, 40-Fe^{3+}-DCPD, and 50-Fe^{3+}-DCPD and in Fe^{3+}-DCPD) were measured using the peak broadening analysis from X-ray diffraction using the Debye-Scherrer equation:

$$D = \frac{K\lambda}{\beta\cos(\theta)} \qquad (1)$$

In equation 1, D stands for the crystallite size (nm), K is a shape factor constant ~0.9, λ for the wavelength (0.154 nm), β illustrates the half-width of the diffraction band (FWHM) (radians), and (θ) is the Bragg-diffraction angle (peak positions in radians).

The Hitachi SU8230 1–30 kV cold field emission gun SEM (Düsseldorf, Germany) was used to examine the morphology of the fabricated freeze-dried unloaded and Fe^{3+}-DCPD mineral-loaded scaffolds. The samples were coated with 6 μm of iridium before SEM analysis to minimize the charging of the surface to improve image contrast. The SEM micrographs were processed and analysed using ImageJ software (version 1.41 USA).

2.3 Bulk Property Analysis of Freeze-Dried Materials

Zeta potential measurements were performed using the Melvern Zetasizer instrument. The Fe-DCPD minerals and chitosan had refractive indices of 1.65 and 1.52, respectively.

From each group of compositions, the test pieces (n=3) of freeze-dried scaffolds (CH, 20-Fe^{3+}-DCPD, 30-Fe^{3+}-DCPD, 40-Fe^{3+}-DCPD, and 50-Fe^{3+}-DCPD) were mechanically tested using the Instron 5569 machine, USA. The sample dimensions were 5x1cm ^{2,} were positioned between polystyrene segments to avoid slippage, and were tested using a 100N load at 100 mm/min strain rate.

Freeze-dried scaffolds (n=3) were dried in a furnace for 24 hrs at 60 °C and weighted (Wo) then soaked in PBS for 4 weeks at 37 °C. Each scaffold was removed from PBS (PBS, Life Technologies, Paisley, UK) every week, dried in an oven at 60°C for 24 hrs, and then weighed to record the weight change. After each record of weight change, the sample was placed again in a fresh PBS solution. The percentage loss in weight was calculated using Equation (2).

$$Degradation\ \% = \frac{Wo - Wd1}{Wd1} * 100 \qquad (2)$$

Wo is the scaffold's initial weight, and $Wd1$ is the scaffold weight at time (t).

Before the experiment, the scaffolds were dried and weighed (Wd) at 60 °C for 24 hrs. The samples of freeze-dried scaffolds were immersed in the PBS solution for 30 minutes at 37°C using separate Eppendorf tubes, after which each sample was removed from the PBS medium and dried using Whatman Grade 44 filter paper. The filter-paper dried samples were then reweighed on an electronic scale to characterize the swelling characteristic using an identical approach, explained in eq.2. Using equation 3, the swelling percentage for each group (n=3) was determined. using Equation (3).

$$Swelling\ \% = \frac{Ww - Wd}{Wd} * 100 \qquad (3)$$

W_w represents the scaffolds' wet weight, and W_d is the dry weight of the scaffolds.

2.4 *In Vitro* Testing

In vitro, studies were conducted with fabricated freeze-dried scaffolds (CH, 20-Fe^{3+}-DCPD, 30-Fe^{3+}-DCPD, 40-Fe^{3+}-DCPD, and 50-Fe^{3+}-DCPD) with a diameter of 5 mm and a height of 2.5 mm. All samples were sterilised using 70 (v/v) % ethanol and then washed thrice with PBS.

The Leeds General Infirmary was granted ethical authorisation by the Yorkshire and Humberside National Research Ethics Committee to obtain human tissue samples (ethics reference 06/Q1206/127 for bone marrow aspirate (BMA)) from hip replacement patients. The cells were cultured to generate plastic adherent bone marrow mesenchymal stem cells (MSCs). Once confluent, the cells were frozen using 10 % DMSO from Thermo Scientific in Loughborough, UK, in 45 % Dulbecco's Modified Eagle Medium (DMEM), Life Technologies, Paisley, UK, and 45 % foetal bovine serum (FBS), Thermo Scientific, Loughborough, UK. For *in vitro* cytotoxicity testing, cells frozen vials from three donors were defrosted, pooled, and cultured to passage 3 (p3) in complete MSC StemMACS media (SM) (Miltenyi Biotec, Bisley, UK). Cells were seeded in T25 flasks (Corning, New York, NY, USA) at a density of 2 x 10^5 and incubated at 37°C and 5 % CO_2 until almost confluent and ready for use. Half of the media change twice weekly was done to sustain the cultures. After detaching the cells, the flasks were rinsed with DPBS and treated with 5 mL of Trypsin/ethylene diamine tetra acetic acid (EDTA) from Sigma (Poole, UK) for 5-7 minutes at 37°C. Then, 15 mL of DMEM with 10 % FBS was added to the flask to cease trypsin activity. A 20 mL cell culture was centrifuged at 1800 rpm for five minutes to produce a pellet. Cells were resuspended in full DMEM media and counted with trypan blue.

Direct Cytotoxicity tests: Sterilised scaffold samples (n=2) were placed into a 6-well plate and secured with steri-strips (3 M steri-strips, Medisave, UK). Following a seven-day ISO10993-5:2009 protocol, 50,000 cells/well in 2 ml StemMACS were introduced to each well, with a control group comprising just cells without scaffolds with StemMacs. At one, three, and seven days, microscopic ((EVOS, ThermoFisher Scientific, USA) images of scaffold/cell interfaces were obtained.

Indirect Cytotoxicity: Scaffold eluates were prepared from all types of scaffolds (n=2 from each scaffold type) according to the ISO standard: ISO 10993-12:2007 part 12. Each sterile scaffold was placed in 6-well plates with 3 ml of SM medium per well for obtaining the sample eluates. The plates were then incubated for 72 hours, 7 days, and 14 days at 37 °C and 5 % CO_2. On the day of extract collection, 330 μL of media was collected in 6 Eppendorf tubes from each scaffold. The test settings comprised a positive control (SM), a negative control (10 % DMSO in SM), and duplicate extracts from each scaffold. Once the eluate was prepared, cytotoxicity was evaluated according to ISO: 10993-5:2009 (E) part 5: Tests for *in vitro* cytotoxicity.

The fabricated freeze-dried scaffolds (Fe^{+3}-DCPD mineral-free chitosan and different amounts of Fe-DCPD-loaded chitosan scaffolds) were performed in two parts. These are indirect cytotoxicity and cell proliferation by XTT ((2,3-bis-(2-methoxy-4-nitro-5-sulfophenyl)-2H-tetrazolium-5-carboxanilide)) Assay.

Indirect Cytotoxicity by XTT Assay: Three MSCs (n = 3) were pooled and placed in a 96-well plate with 200 μL of SM medium at 1 x 10^4 cells per well for 24 hrs. After 24 hrs, the medium was replaced with 100 μL of defrosted extracts containing the scaffold eluate, negative control, or positive control for another 24 hrs before the addition of XTT reagents, as explained below.

Proliferation assay by XTT assay: Three different MSCs were seeded in duplicate (for each scaffold, n=2 samples were used) of a 96-well plate in 200 µL of SM at 500 cells/well for 24 hrs. After 24 hrs incubation, the basal media was removed and replaced with 100 µL/well containing either the scaffold eluate, negative or positive control. Then, the pellet was put in the incubator at 37 °C for 4 days. After four days, the XTT test was performed as indicated above, and the cell proliferation was quantified compared to the positive control.

XTT Assay: XTT cell proliferation assays were performed according to the manufacturer's instructions. Briefly, 5 mL of XTT labelling reagent (Sigma, Dorset, UK) was mixed with 0.1 mL of electron coupling reagent in a 96-well microplate. Following that, media in wells (scaffold extract, positive or negative control medium) was removed and replaced with 100 μL of DMEM with 10 % FBS and 50 μL of XTT solution and incubated at 37°C for 4 hours. The aliquots from each well were transferred to a new plate and read using a microplate reader (Cytation 5, Biotek) at 450 and 630 nm (reference wavelengths). The optical density (OD) was estimated by subtracting the reference wavelength (630 nm) from 450 nm. Cell viability or proliferation inhibition was measured by normalising the ODs of test wells to those of the positive control.

2.5 Statistical Analysis

Data from *in vitro* experiments were analysed using Graph Pad Prism (version 9.5.0). The data was analysed using two-way ANOVA with Geiser greenhouse correction. Matching values were stacked across a row in the datasheet. Multiple comparisons were conducted to determine the percentage of viable cells for each scaffold type at each time point.

3. Results

3.1 Characterisation Results

Raman Spectroscopy: The Raman spectroscopic analysis data show the characteristic vibration bands associated with the functional groups in Fe^{3+}-DCPD mineral, mineral-free chitosan (CH) and mineral-loaded chitosan freeze-dried scaffolds (20, 30, 40, and 50-Fe^{3+}-DCPD). Figure 1 illustrates the Raman spectra of the freeze-dried materials. The Fe^{3+}-DCPD mineral exhibits significant phosphate $(PO_4)^{3-}$ vibrational modes (Figure 1 (a)) [29]. The P-O symmetric stretching of the PO_4^{3-} ion corresponds to the vibrational mode, which has its highest frequency at 988 cm^{-1}. The antisymmetric Raman HPO_4^{2-} vibration bands are located at 882 and 1147 cm^{-1}. The lower frequency $(PO_4)^{3-}$ vibrations are often seen between 385 and 420 cm^{-1}, whereas the frequencies between 436 cm^{-1} and 590 cm^{-1} correspond to symmetrical bending of P-O bonds. The vibrational structural analysis demonstrates that the addition of Fe^{2+}/Fe^{3+} ion substitution in DCPD does not change the structure of DCPD which is in agreement with similar Raman findings for Fe^{3+}-DCPD and DCPD reported in the literature [26,29]. All fabricated freeze-dried scaffolds have exhibited -NH_2 symmetric and asymmetric stretching from 3200 cm^{-1} to 3450 cm^{-1} corresponding to CS structure as part of the N-acetyl glucosamine units. The broad -OH stretching is visible between 3100 cm^{-1} and 3400 cm^{-1}, whereas the -CH stretching is present between 2880 cm^{-1} and 2990 cm^{-1}. The Raman spectra of mineral-loaded freeze-dried scaffolds are comparable with those of freeze-dried CS scaffolds (Figure 1 (b-d)); however, there is a considerable difference in peak broadenings and intensities in the 2800 cm^{-1} and 3800 cm^{-1} regions. As reported previously [30], the lack of crystallinity of the mineral phase is proportional to the Fe^{3+}-DCPD concentration incorporated during the synthesis process which we have also verified using the X-ray powder diffraction analysis below. For all Fe^{3+}-DCPD, the Raman peaks in Figure 1 (b-d), both below and above 2000 cm^{-1} wave numbers, are significantly broadened which suggests that the presence of Fe^{3+}-ions in DCPD structure not only changes the P-O bonding with Ca^{2+} but also introduces more complex (Ca^{2+}-PO_4^{3-}—$Fe^{2+,3+}$) interaction, resulting into a larger distribution of (PO_4^{3-}) vibrational states than without the presence of $Fe^{3+,2+}$ ions. In addition, the vibrational bands for OH^- (2800-3000 cm^{-1}) and the CH- and -NH_2 groups are also broadened, as shown in Figure 1(c) and (d). The wider energy distribution of Raman vibrational states confirms that the inorganic phosphate groups are dispersed with the molecular functional groups of chitosan during the synthesis and freeze-drying process. The distribution of vibrational energy of molecular states in the mineralized chitosan confirms that the mineral-chitosan suspension before freeze-drying may also be amenable to changes in the consequential rheology, which we have characterized by determining the zeta potential data below.

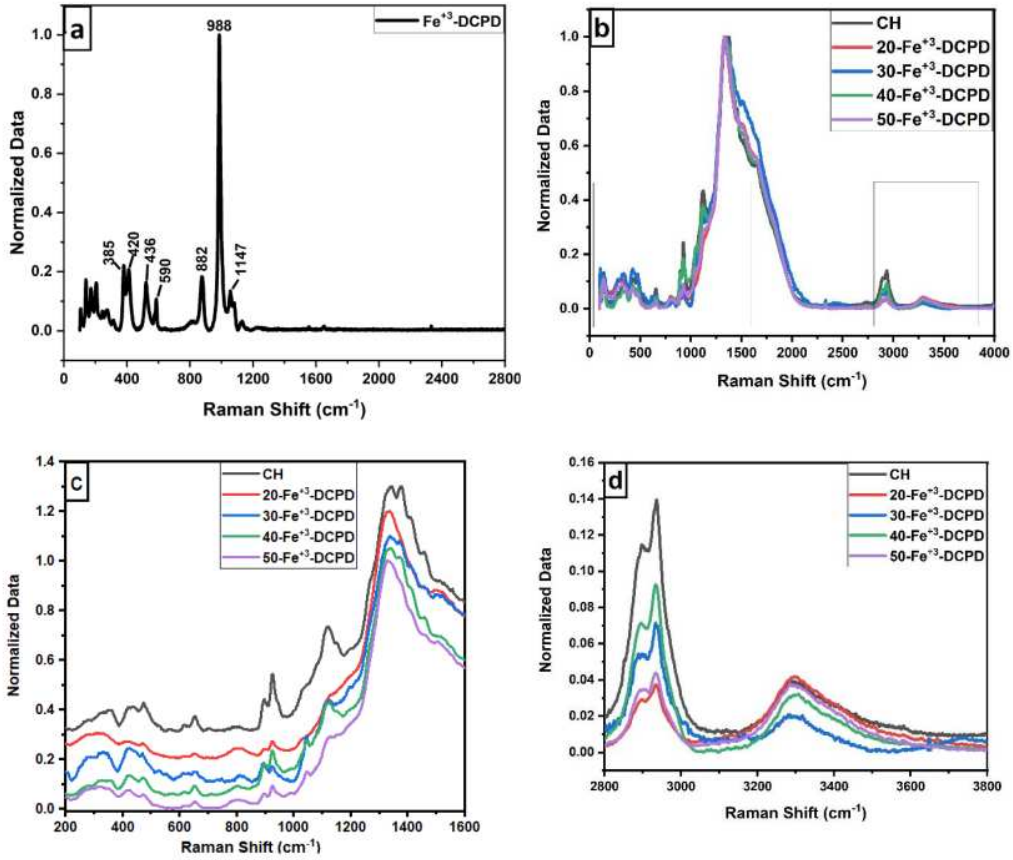

Figure 1- Normalised Raman Spectra for the following: (a) Fe-Dicalcium Phosphate Dihydrate mineral (Fe^{3+}-DCPD mineral) powder; (b) comparison of the various Fe^{3+}-DCPD mineral concentrations (0, 20, 30, 40, and 50 (wt) %) loaded chitosan fabricated freeze-dried scaffolds in the range of 100 to 4000 cm^{-1}; (c) 200 to 2800 cm^{-1} region with 0.2 offsets; and (d) 2800 to 3800 cm^{-1}.

3.2 Fourier Transform Infrared Spectroscopy

The FTIR data for fabricated Fe^{3+}-DCPD mineral, the unloaded and the Fe^{3+}-DCPD mineral-loaded chitosan scaffolds are compared in Figure 2(a,b). The FTIR vibration bands 520 cm^{-1}, 980 cm^{-1}, and 1050 cm^{-1} are associated with PO_4^{3-} contributions associated with Fe^{3+}-DCPD minerals. The bands corresponding to the HPO_4^{-2} are located at 860 cm^{-1}, 1120 cm^{-1}, and 1180 cm^{-1} which are consistent with the data in the literature [30]. The freeze-dried chitosan scaffolds exhibit a broad transmission band at 3291 cm^{-1} and 2993 cm^{-1}, corresponding to N-H and O-H stretching, respectively. The peak at 2921 cm^{-1} corresponds to CH_2 symmetric and asymmetric stretching, these bands are polysaccharide typical characteristics [31]. The backbone conformation is closely connected to the amide stretching vibration C=O (amide I) at 1645 cm^{-1}, whereas the C-N stretching vibration (amide III) is at 1325 cm^{-1}. The N-H bending vibration (amide II) occurs at 1550 cm^{-1}. The appearance of bands at 1375 cm^{-1} is assigned to the CH_3 symmetrical deformations, whereas the 1589 cm^{-1} corresponds to the bending vibration of the primary amine N-H bending. The asymmetric stretching of the C-O-C, which is dependent on the crystallinity of chitosan, is responsible for the absorption band

at 1153 cm^{-1} [32–36]. The Fe^{3+}-DCPD mineral-loaded freeze-dried scaffolds have FTIR spectra identical to the CS scaffold and can be explained by the HPO_4^{2-} and PO_4^{3-} peaks associated with the Fe^{3+}-DCPD mineral, which also overlap with the chitosan amide (I, II, and III), CH_3, and saccharide bands. The Fe^{3+}-DCPD mineral phosphate groups (trivalent PO_4^{3-} and divalent HPO_4^{2-}) and the protonated chitosan amino groups (NH_3^+) have been shown to produce strong intermolecular interactions [14]. Additionally, the calculated areas of the amide I, II, and III peaks are shown in Figure 2(b), where a noticeable trend reduction in area is observed with increasing concentrations of Fe^{3+}-DCPD minerals. As the mineral ratio rises, the divalent $(HPO_4)^{2-}$ and trivalent $(PO_4)^{3-}$ groups increase the potential of interaction with protonated CS amino groups, resulting in Coulombic ionic crosslinking which then reduces the available molecular vibration states and, therefore, the overall peak areas are proportionately reduced [37].

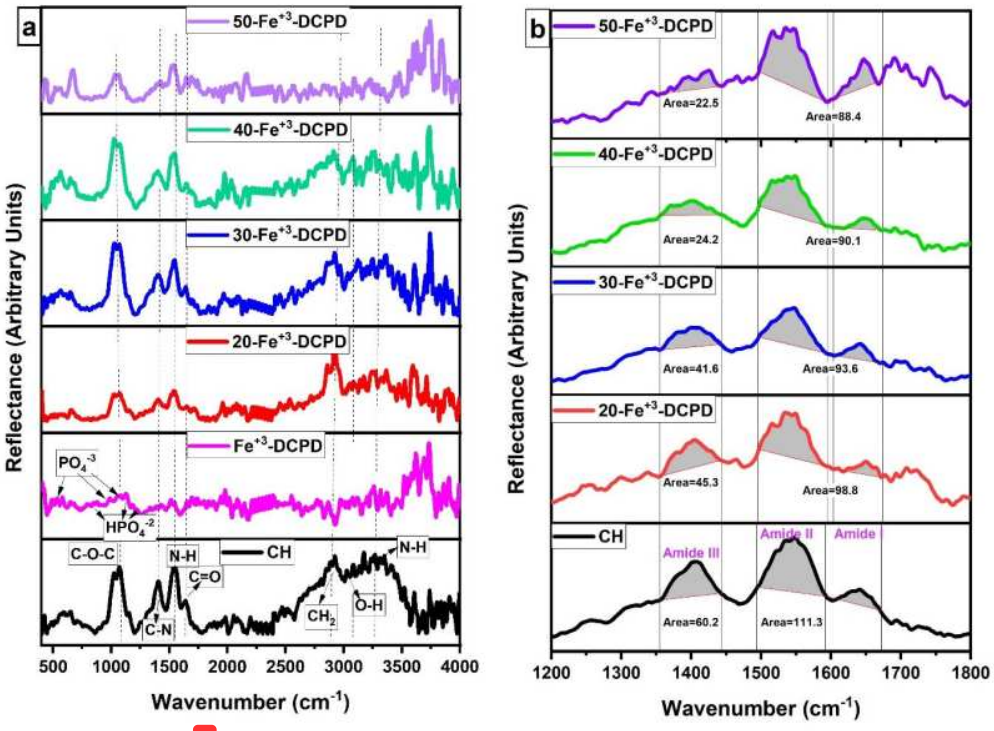

Figure 2- Fabricated freeze-dried chitosan scaffolds were compared with different concentrations of the 10 (mol)% Iron (III) nitrate doped Dicalcium Phosphate Dihydrate (Fe^{3+}-DCPD) mineral (CH, 20, 30, 40, and 50- Fe^{3+}-DCPD). (a) Data were acquired using the Vertex 70 FTIR spectrometer in attenuated total reflection (ATR) mode, between 400 and 4000 cm^{-1}, with a resolution of 4 cm^{-1}, (b) Amide I, II, and III peak comparison.

3.3 X-Ray Diffraction (XRD)

The experimental XRD diffraction data for the synthesised Fe^{3+}-DCPD minerals and freeze-dried scaffolds (CH, 20-Fe^{3+}-DCPD, 30-Fe^{3+}-DCPD, 40-Fe^{3+}-DCPD, and 50-Fe^{3+}-DCPD) are compared in Figure 3. Only DCPD peaks were found in a material doped containing 10 (mol) % iron (III) nitrate [26], suggesting no mineral contamination. The Fe^{3+}-DCPD pattern's peaks

are comparable with the XRD data for DCPD assembled by the Joint Committee on Powder Diffraction and Standards (JCPDS ref: 00-011-0293). The primary 2Θ peaks for the Fe^{3+}-DCPD standard are 11.60°, 23.39°, 29.16°, 35.45°, and 47.84°, corresponding to the crystallographic planes (020), (040), (-112), (-231), and (080). Two dominant phases found were DCPD and iron-complexed calcium phosphate mineral, reported elsewhere [26].

The partially crystalline polysaccharide CS exhibits a characteristic XRD fingerprint, comprising two broad peaks at ~10° and ~20°, which relate to the crystal I and II phase forms, respectively [38]. The less hydrated crystal I phase exhibits higher crystallinity. On the other hand, the more hydrated crystal II phase has an amorphous form that indicates the intermolecular interactions between the aligned CS polymer chains. The Fe^{3+}-DCPD is a highly crystalline mineral because of the $Fe^{3+,2+}$-ion interactions with $(HPO_4)^{2-}$ and $(PO_4)^{3-}$ anions in the DCPD lattice. As a result, a considerable reduction in the CS crystal II phase was observed in all the freeze-dried scaffolds containing the Fe^{3+}-DCPD mineral. The diffraction patterns of the freeze-dried scaffold (20, 30, 40, and 50-Fe^{3+}-DCPD) reveal evidence of a semi-crystalline CS matrix, in addition to the typical crystalline diffraction peaks associated with Fe^{3+}-DCPD minerals. The CS phase in Figure 3(a) appears partially crystalline which becomes progressively more crystalline as the Fe^{3+}-DCPD concentration increases in the freeze-dried scaffold.

Using Scherrer's Equation 1, the X-ray line broadening data in Figure 3(a) were analysed to determine the average crystallite size present in the freeze-dried scaffolds. As can be seen in Figure 3(c), the average crystallite size increased as the concentration of Fe^{3+}-DCPD mineral increased.

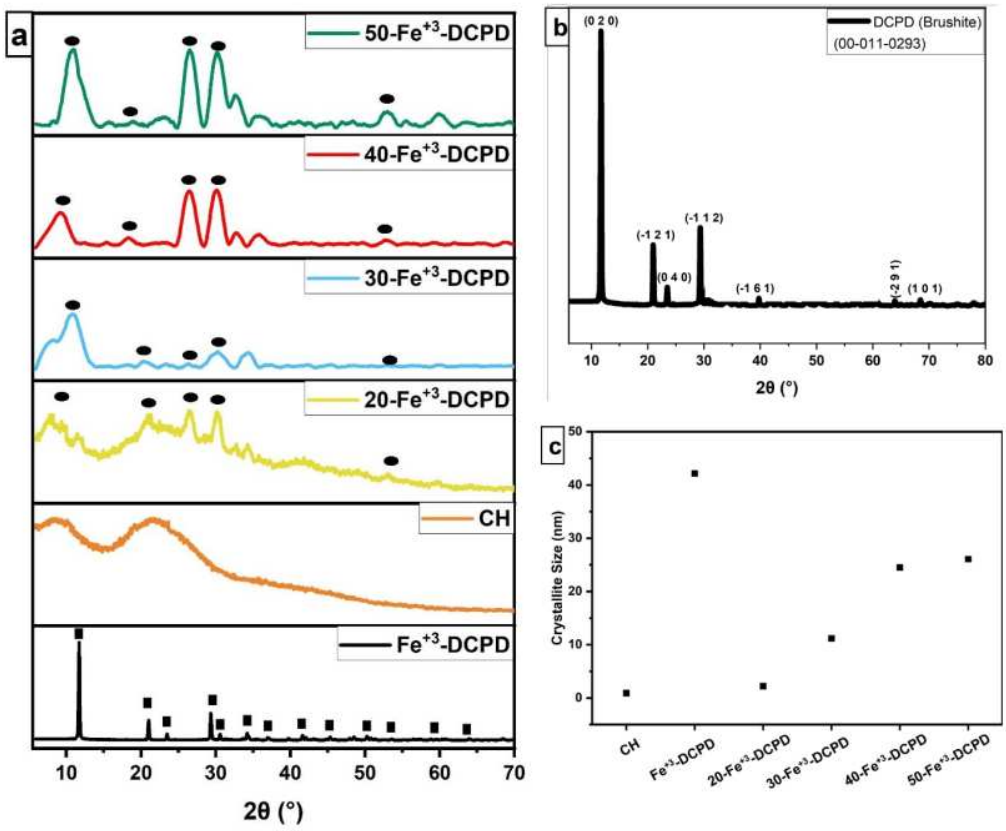

Figure 3- Normalised X-ray diffraction data, (a) Experimental XRD spectra for synthesised Fe-DCPD mineral, mineral-free CH, and different amounts of Fe^{3+}-DCPD-doped chitosan (20, 30, 40, and 50-Fe^{3+}-DCPD) freeze-dried scaffolds, (b) DCPD reference spectra (JCPDS), and (c) crystallite size comparison. '■' corresponds to the Bragg 2Θ diffraction peaks of Fe^{3+}-DCPD with miller indices (0 2 0), (0 4 0), (-1 1 2), (-2 3 1), and (0 8 0), respectively.

3.4 Scanning Electron Microscopy (SEM) and Energy Dispersive X-Ray (EDX)

The microstructures of CH, Fe^{3+}-DCPD and Fe^{3+}-DCDP doped chitosan were investigated using SEM images in Figure 4(b-d). As shown in Figure 4(b-d), with increasing Fe^{3+}-DCPD concentration, the shape and structural features of the scaffolds change. The mineral-free CH scaffold shows thick lamellae with pores ranging from 20 μm to 180 μm. The incorporation of Fe^{3+}-DCPD minerals reduced the inter lamellae pore size distribution and their thickness. The structural alteration and increased number of pores are visible compared to the 20-Fe^{3+}-DCPD and 30-Fe^{3+}-DCPD scaffolds. In Figure 4(e and f), the structure of pores and lamellae are shown for 40-Fe^{3+}-DCPD and 50-Fe^{3+}-DCPD, respectively, confirming the reduction in the average size of pores and size of lamellae, which led to the consequential loss of interconnected pores.

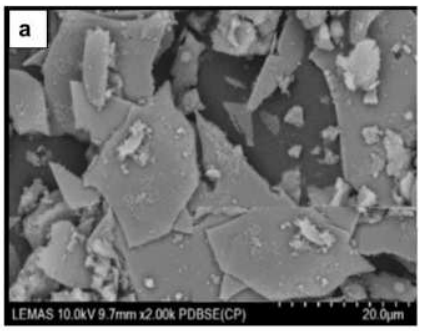
a
LEMAS 10.0kV 9.7mm x2.00k PDBSE(CP)
20.0µm

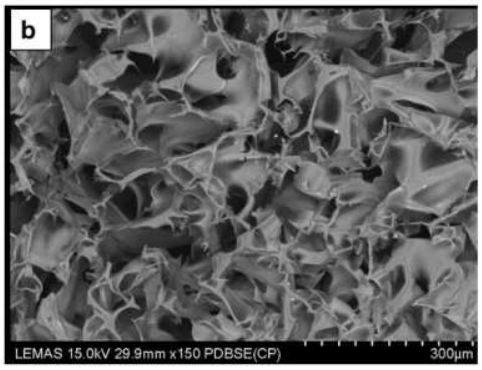
b
LEMAS 15.0kV 29.9mm x150 PDBSE(CP)
300µm

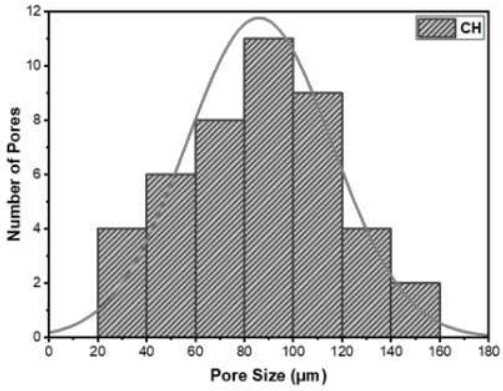
CH
Number of Pores
Pore Size (µm)
0
2
4
6
8
10
12
0
20
40
60
80
100
120
140
160
180

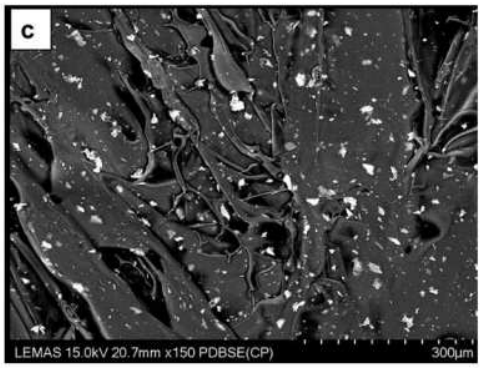
c
LEMAS 15.0kV 20.7mm x150 PDBSE(CP)
300µm

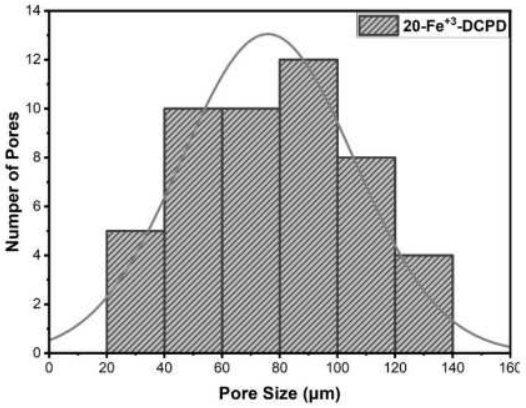
20-Fe+3-DCPD
Numper of Pores
Pore Size (µm)
0
2
4
6
8
10
12
14
0
20
40
60
80
100
120
140

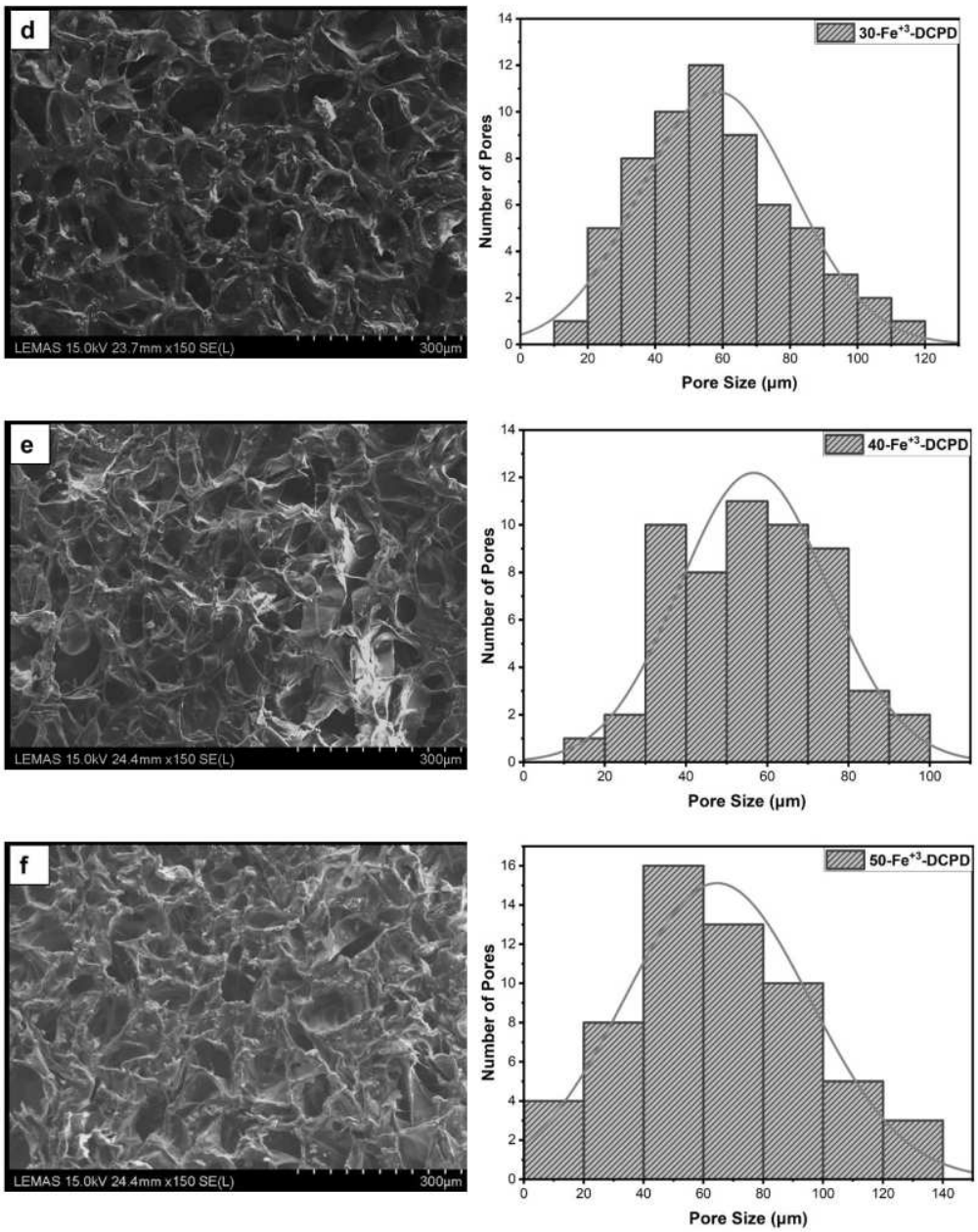

Figure 4 The Hitachi SU8230 SEM image results of (a) 10 (mol) % iron (III) nitrate doped Dicalcium Phosphate Dihydrate (Fe^{3+}-DCPD) mineral, (b) freeze-dried chitosan (CS), (c) 20- Fe^{3+}-DCPD, (d) 30- Fe^{3+}-DCPD, (e) 40- Fe^{3+}-DCPD, and (f) 50- Fe^{3+}-DCPD.

The surface elemental analysis results of the fabricated freeze-dried mineral unloaded and loaded chitosan scaffolds (CH, 20- Fe^{3+}-DCPD, 30- Fe^{3+}-DCPD, 40- Fe^{3+}-DCPD, and 50- Fe^{3+}-DCPD) are demonstrated in Figure 5(a-e). The EDX analysis was used to examine mineral distributions and how increasing amounts of minerals affected pore size. It was found that the

distribution of minerals on the surface increased with increased mineral concentration, resulting in varying pore sizes for the samples.

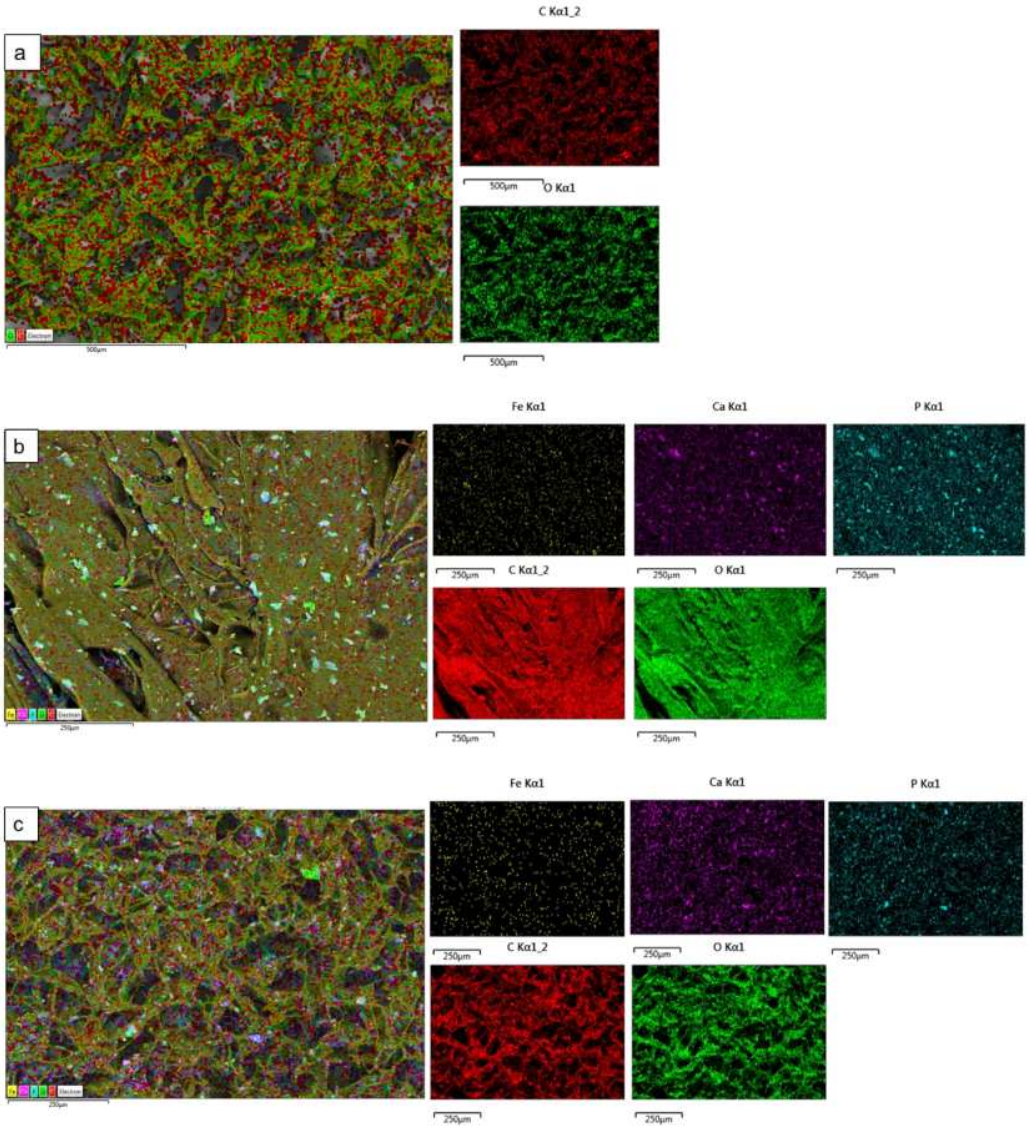

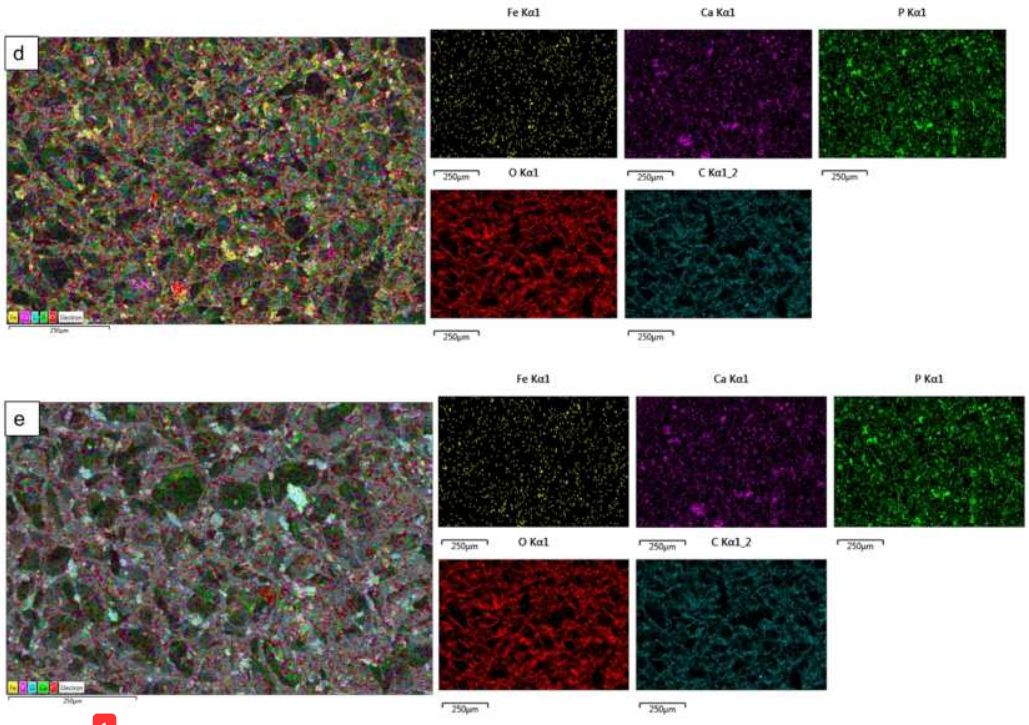

Figure 5- The Hitachi SU8230 SEM with a dispersive energy X-ray (EDX) detector was used to analyse the surface elemental characterization of freeze-dried chitosan scaffolds without Fe^{3+}-DCPD mineral and with various Fe^{3+}-DCPD mineral concentrations (20, 30, 40, and 50 (wt) %). Freeze-dried (a) Chitosan, (b) 20- Fe^{3+}-DCPD, (c) 30- Fe^{3+}-DCPD, (d) 40- Fe^{3+}-DCPD, and (e) 50- Fe^{3+}-DCPD scaffold.

3.5 Zeta Potential

The stability of a suspension is characterised by the Zeta potential, which measures the potential due to surface charge around the solid surface in colloidal dispersions [39]. The Zeta potential of the Fe^{3+}-DCPD mineral was found to be -10.53±0.41 mV, implying that it was aggregated, as confirmed by SEM analysis in Figure 4(a). The negative surface charge density relates to the presence of phosphate groups (PO_4^{3-}) terminating at the surface of solids.

All the freeze-dried chitosan scaffolds were found to have positive zeta potential values, indicating amino group protonation. Although the magnitude of the potential decreased with the increasing proportion of Fe^{3+}-DCPD mineral, the average zeta potential for CH (mineral-free) and 50- Fe^{3+}-DCPD mineral-loaded freeze-dried scaffolds decreased from +48.6 ± 0.4 mV to +21.6 ± 0.41 mV, as shown in Table 2. The interaction between the protonated CH scaffold amino groups ($-NH_3^+$) and the Fe^{3+}-DCPD phosphate groups (PO_4^{3-}) is likely the reason for the reduction in the overall magnitude of positive potential.

Table 2- Zeta potential values for the mineral Fe^{3+}-DCPD, chitosan, and various concentrations of Fe-DCPD-loaded chitosan scaffolds.

Sample	Zeta Potential (mV)	Standard Deviation
CH	+48.6	0.4

Fe^{3+}-DCPD	-10.53	0.41
20- Fe^{3+}-DCPD	+40.6	0.39
30- Fe^{3+}-DCPD	+37.53	0.31
40- Fe^{3+}-DCPD	+30.6	0.7
50- Fe^{3+}-DCPD	+21.6	0.41

3.6 Mechanical Test

Table 3 shows the mechanical test results of scaffolds with Fe^{3+}-DCPD mineral and chitosan. With increasing Fe^{3+}-DCPD concentrations led to a proportionate increase in Young's modulus and tensile strength, when compared with mineral-free CH scaffolds. Scaffolds with smaller average pore diameters exhibited better mechanical characteristics because of the reduced pore volume and increased crystalline fractions.

Table 3- The Instron 5569 machine mechanical test results of freeze-dried mineral-free and different concentrations of Fe^{3+}-DCPD mineral-added chitosan scaffolds (0, 20, 30, 40, and 50 (wt) %, n = 3 samples were used for each type of scaffold).

	CH	20- Fe^{3+}-DCPD	30- Fe^{3+}-DCPD	40- Fe^{3+}-DCPD	50- Fe^{3+}-DCPD
Youngs Modulus (kN/m^2)	5.4 ± 0.19	10.3 ± 0.04	24.7 ± 0.3	30.1 ± 0.51	31.3 ± 0.06
Tensile Strength (kPa)	7.4 ± 0.18	11.4 ± 0.35	29.9 ± 0.28	31.3 ± 0.04	34.9 ± 0.03

3.7 Degradation of Scaffolds

The fabricated freeze-dried mineral-free (CH) and different concentrations of Fe^{3+}-DCPD mineral (20, 30, 40, and 50 (wt) %) loaded chitosan scaffolds were analysed for degradation as shown in Figure 6. The observed patterns show an initial fast degradation rise from 0 to 1st week for all scaffolds. Between the 1st and 3rd weeks, there was a gradual rise, followed by a decrement of degradation rate between 3 and 4 weeks. With increasing Fe^{3+}-DCPD concentration, the rate of mass loss was found to decrease with increasing proportion of Fe^{3+}-DCPD; the lowest mass loss was found to be 20.5 ± 3.8 % for 50-Fe^{3+}-DCPD. The degradation rate for CH and other mineral-bearing scaffolds is compared in Figure 6.

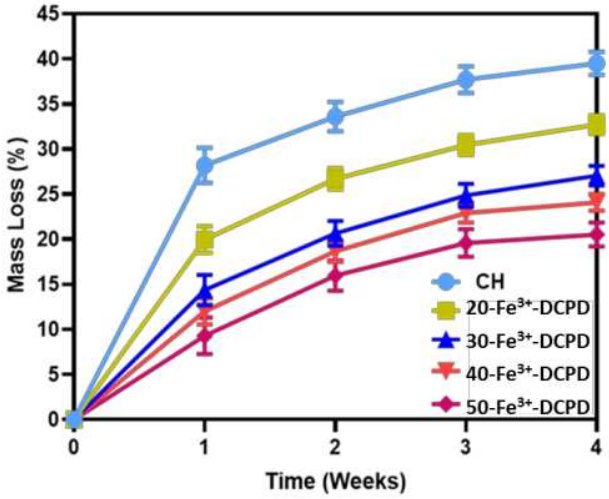

Figure 6- Mineral-free and different concentration Fe^{3+}-DCPD mineral embedded chitosan freeze-dried scaffolds degradation results (CH, 20, 30, 40, and 50- Fe^{3+}-DCPD) when they are dissolved in phosphate saline buffer (pH 7.4) at 37 ˚C. Over 4 weeks, the studies were performed in triplicate. The error bars demonstrate each group's standard deviation (SD) ± mean, n = 3.

3.8 Swelling of Scaffolds

The ability of a scaffold to retain water is a crucial factor in assessing its feasibility for tissue engineering. The swelling properties of scaffolds have been demonstrated to considerably affect cell adhesion, growth, and differentiation [40]. Figure 7 compares the swelling behaviour of freeze-dried CH scaffolds with varying Fe^{3+}-DCPD mineral concentrations across time intervals. The observed patterns reveal a rapid increase in swelling from 0 to 30 minutes for all scaffolds. A slow increase occurs between 30 and 180 minutes, followed by mass stability between 180 and 300 minutes. The swelling percentage varies from 783 ± 27.3 % for Fe^{3+}-DCPD mineral-free CH freeze-dried scaffolds to 475.4 ± 21.8 % for 50- Fe^{3+}-DCPD mineral freeze-dried scaffolds, demonstrating a considerable influence of Fe^{3+}-DCPD mineral concentrations on swelling.

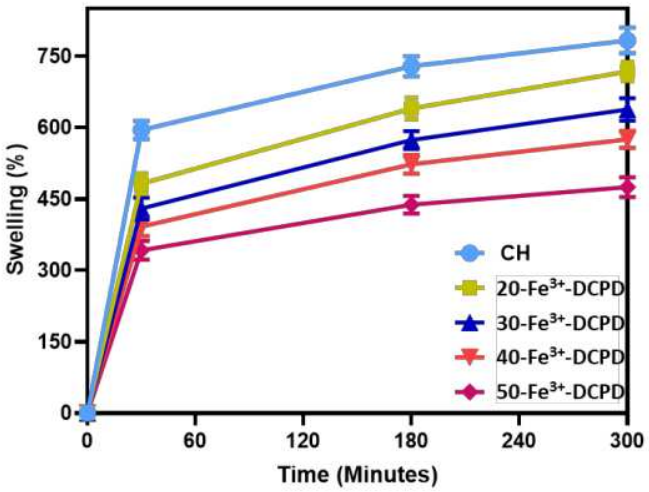

Figure 7- The swelling kinetics of mineral-free chitosan (CH), 20, 30, 40 and 50- Fe^{3+}-DCPD freeze-dried scaffolds immersed in phosphate saline buffer (pH 7.4) at physiological temperature 37 °C. Experiments were carried out in triplicates for each of the fabricated scaffolds. The error bars represent the mean ± standard deviation (SD) for n = 3 in each group.

3.9 *In Vitro* Cell Results

3.9.1 Direct Cytotoxicity

Direct cytotoxicity assay testing is a qualitative evaluation of cytotoxicity that uses microscopic observations to examine the MSC cell shape and environment of media, exhibiting changes in the media's colour (ISO10993-5:2009). Figure 8 demonstrates the 7-day direct cytotoxicity results. On days 1, 3, and 7, images of the control well with MSCs and the fabricated freeze-dried scaffolds (CH, 20-Fe^{3+}-DCPD, 30-Fe^{3+}-DCPD, 40-Fe^{3+}-DCPD, and 50-Fe^{3+}-DCPD) were taken. After day 7, the media's colour remained stable, and there was no turbidity, indicating that the cells were healthier than the control MSCs. Moreover, the morphology of the cells at the cell-scaffold interface did not change and remained consistent with the control, indicating that the scaffolds were not cytotoxic to MSCs.

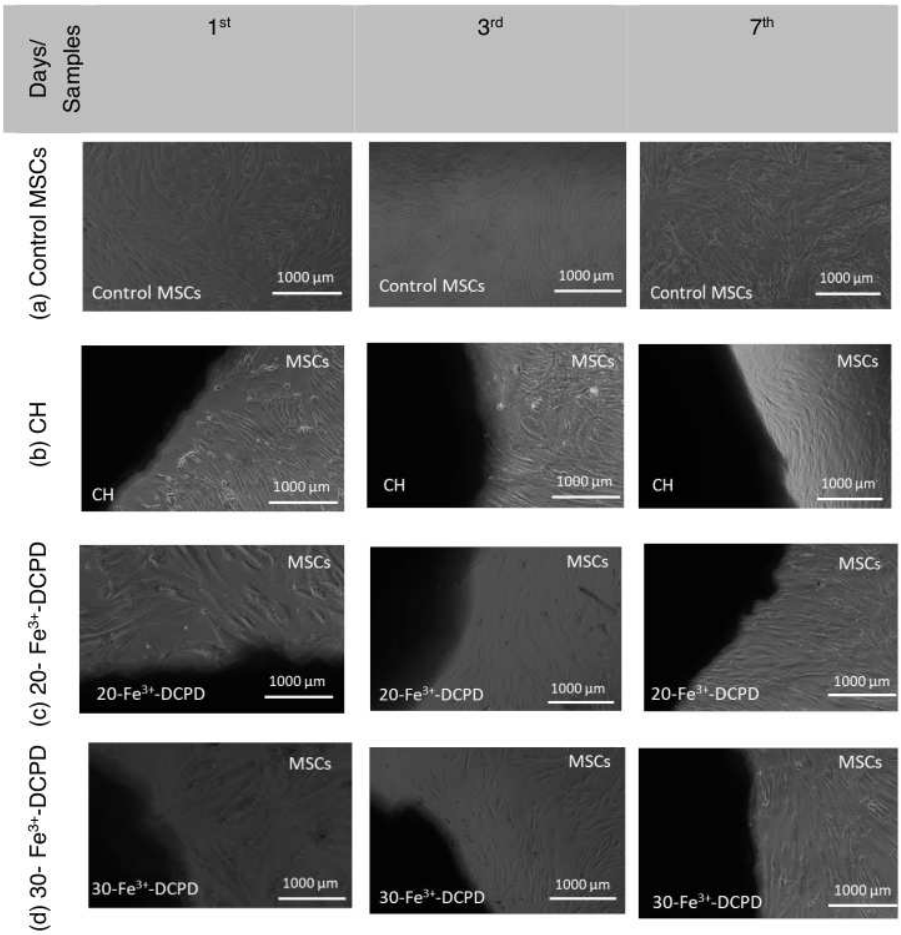

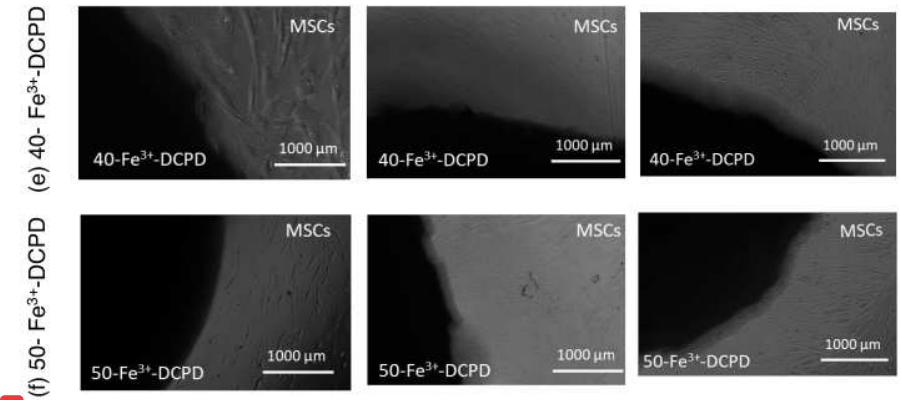

Figure 8- Direct cytotoxicity. Images of chitosan freeze-dried scaffolds with varied Fe^{3+}-DCPD concentrations (0, 20, 30, 40, and 50 (wt) %) were obtained at x4 on the first, third, and seventh days. (a) Control MSCs, which were bone marrow mesenchymal stem cells (MSCs) without scaffolds, (b) mineral-free CH scaffold, (c) 20- Fe^{3+}-DCPD, (d) 30- Fe^{3+}-DCPD, (e) 40- Fe^{3+}-DCPD, and (f) 50- Fe^{3+}-DCPD.

3.9.2 Indirect Cytotoxicity

Indirect Cytotoxicity by XTT Assay: The indirect cytotoxicity findings of the freeze-dried CH and 20, 30, 40, and 50 (wt) % Fe^{3+}-DCPD doped chitosan scaffolds (Figure 9) showed greater than 80 % cell viability at all periods, namely 3, 7, and 14 days. The indirect cytotoxicity results for freeze-dried scaffolds show that the extract obtained from the scaffolds is non-toxic and has higher viability compared to the positive control. It demonstrates that the Fe^{3+}-DCPD mineral did not inhibit the cell. There were no significant differences between the percentage of living cells exposed to both scaffold extract and the positive control MSCs. Furthermore, the findings reveal that all Fe^{3+}-DCPD scaffolds promoted MSCs.

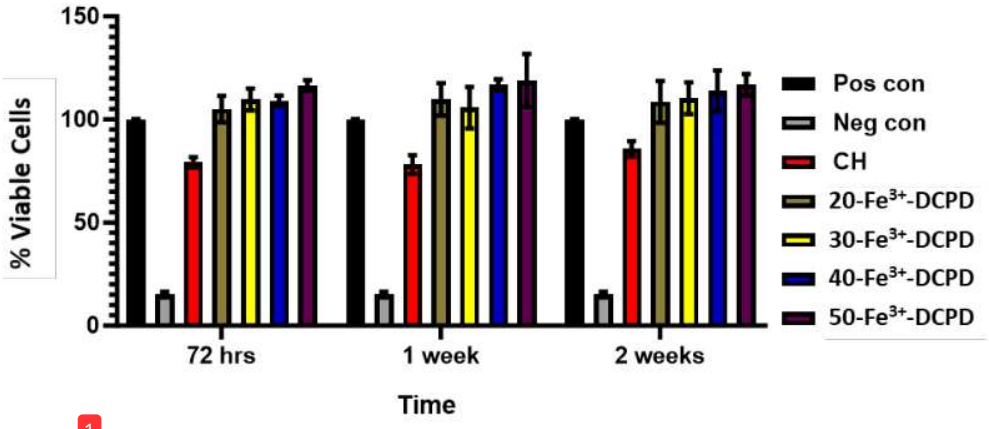

Figure 9- Cytotoxicity by XTT assay test on MSCs exposed to extracts taken from freeze-dried chitosan scaffolds and containing varying concentrations of Fe^{3+}-DCPD minerals (20 (wt)% (20- Fe^{3+}-DCPD), 30 (wt)% (30- Fe^{3+}-DCPD), 40 (wt)% (40- Fe^{3+}-DCPD), and 50 (wt)% (50- Fe^{3+}-DCPD). The error bars represent the mean ± SD (n = 2 in each group).

Cell Proliferation by XTT Assay: The freeze-dried CH and different concentrations of Fe^{3+}-DCPD mineral-loaded (20, 20, 40, and 50 (wt) %) freeze-dried scaffolds results are demonstrated in **Error! Reference source not found.**. The MSCs' proliferative activity was examined using extracts collected for up to 14 days; this was accomplished by exposing the MSCs to the extracts for up to 14 days to allow them to proliferate with positive and negative controls. Cell proliferation results for mineral-loaded chitosan scaffolds (20, 30, 40, and 50-Fe^{3+}-DCPD) are higher than for positive controls, indicating that Fe^{3+}-DCPD minerals do not inhibit cellular growth. Fe^{3+}-DCPD minerals enhance MSC culture, adhesion, and proliferation compared to the mineral-free CH scaffold results for each time point. The porous structure of freeze-dried scaffolds allows for the release of significant minerals to stimulate cellular growth. All Fe-DCPD mineral-loaded chitosan freeze-dried scaffolds (20- Fe^{3+}-DCPD, 30- Fe^{3+}-DCPD, 40- Fe^{3+}-DCPD, and 50- Fe^{3+}-DCPD) exhibit comparable cell proliferation to positive controls at all cell densities. However, compared to the 20, 30, and 40- Fe^{3+}-DCPD scaffolds, the 50-Fe^{3+}-DCPD scaffold had a lower MSC proliferation rate. The SEM results in Figure 4 indicate that the decreased scaffold porosity is most likely causing the lower proliferation.

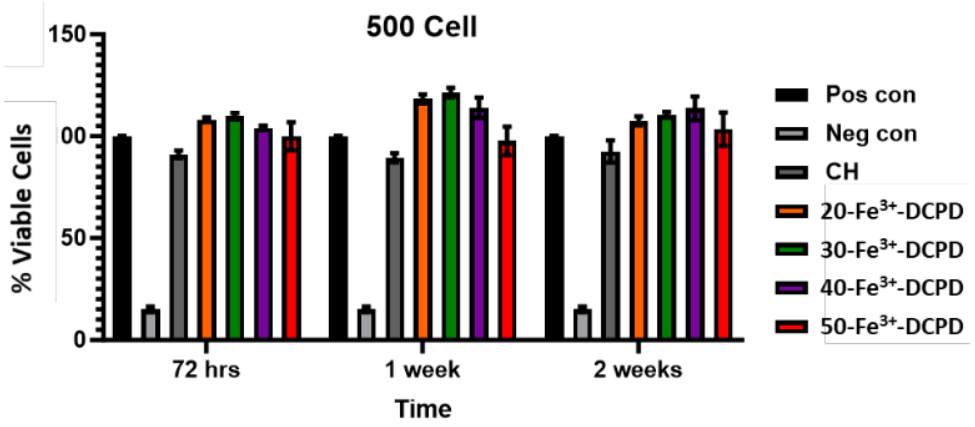

Figure 10- Cell proliferation was assessed using the XTT assay on MSCs exposed to freeze-dried scaffold extracts (CH, 20- Fe^{3+}-DCPD, 30- Fe^{3+}-DCPD, 40- Fe^{3+}-DCPD, and 50- Fe^{3+}-DCPD). The fabricated scaffolds extracts were seeded 500 cells/well. The error bars represent the mean ± SD (n = 2 in each group). There was no significant difference between freeze-dried scaffolds at all time points.

4. Discussion

The fabricated freeze-dried scaffold chemical structure was revealed through Raman and FTIR spectroscopy. Raman peaks of the Fe^{3+}-DCPD [29], and chitosan [41] have been observed similar to the literature. The FTIR results observations for the samples agree with previously reported data [33,35,36,42].

The human bone cancellous part has a complex, porous structure with non-homogeneous anisotropic properties and porosity ranging from 50 to 90 % [40]. The porosity and interconnectivity of the bone scaffold are critical for cell growth and migration, nutrition and waste delivery, and blood vessel invasion [43,44]. In tissue engineering, studies have shown that the average pore size of bone scaffolds ranges from 50 μm to 1500 μm [45,46]. Optimal bone and tissue regeneration requires a minimum pore size range of 50 μm to 100 μm [47–

49]. Pore sizes of 0 to 50 μm create cellular capsules surrounding the scaffold, limiting cellular waste evacuation and nutrition and leading to necrotic regions throughout the structure. Large pores (bigger than 1500 μm), on the other hand, reduce the scaffold surface area, which limits cellular adhesion [43].

The chitosan suspension was frozen at -80°C before freeze-drying since the scaffolds' initial freezing temperatures influence pore size distribution and porosity number. Scaffolds made at -80 °C exhibited a lamellar structure with larger holes, whereas those made at temperatures less than -80 °C had a compact form with smaller pores [50]. Furthermore, the scaffold's freezing rate affects porosity formation. Rapid freezing, such as using liquid nitrogen, results in 91% to 95% porosity. The fast freezing rate results in 13–35 μm pore sizes, which are inadequate for osteoblast development and proliferation [51]. The freeze-drying approach produces bone scaffolds with highly linked porosity structures, as SEM examination results prove. The freeze-dried CH scaffold has the broadest range of pore size. However, when the concentration of Fe^{3+}-DCPD minerals rose, the number of pores increased considerably (Figure 4(b-f)). Pore size distributions reduced, resulting in pore diameters ranging from 20 μm to 140 μm (20- Fe^{3+}-DCPD), 10 μm to 120 μm (30- Fe^{3+}-DCPD), 10 μm to 100 μm (40- Fe^{3+}-DCPD), and 0 μm to 140μm (50- Fe^{3+}-DCPD). Smaller pore diameters (less than 50μm) have been observed that inhibit cell mobility and capsule formation, leading to necrotic regions owing to inadequate nutrition and waste transport [52,53]. Large pores (more than 1500 μm) on the scaffold can limit cell adhesion and reduce its surface area. Scaffolds with high pore diameters also have restricted mechanical properties due to the increased void volume [54–56]. The number of pores associated with the 50- Fe^{3+}-DCPD scaffold decreased considerably (Figure 4(f)). On days 3, 7, and 14, MSC cell growth was reduced compared to the CH, 20, 30, and 40- Fe^{3+}-DCPD freeze-dried scaffolds because most of the pores coalesced, resulting in less defined microstructures with lower pore interconnectivity, as shown in Figure 4. The reduced surface area produced by the loss of individual pores and pore interconnectivity, which most likely resulted in a reduction in the flow of critical nutrients, is likely to induce cell death.

Another essential criterion for assessing a scaffold's suitability for bone tissue engineering is its ability to retain water. The swelling properties of scaffolds have been shown to considerably affect cell adhesion, growth, and differentiation [40]. Synthetic scaffolds with increased water absorption capacities also promote cell adhesion; however, their mechanical properties are often reduced [57]. Chitosan is a natural hydrophilic biopolymer [58] that promotes water molecule diffusion due to its structural free volume and the ease with which polymer chains move [59]. As a result, the Fe^{3+}-DCPD mineral-free CH scaffolds had the highest liquid absorption, but the 50- Fe^{3+}-DCPD scaffolds had the lowest swelling percentage rise. Swelling percentage experiments indicate that all synthesised scaffolds' polymer matrixes can swell and retain water, which is favourable for living tissues [60]. The reduction of hydrophilic functional groups in the cationic CH structure, such as the amine (NH_2) and amide (-CONH, -$CONH_2$) groups, is thought to be responsible for the lower equilibrium swelling % in scaffolds incorporating Fe^{3+}-DCPD mineral [61].

The bone implant biomaterials used should undergo the resorption and degradation process within live tissue. This allows new bone tissue to develop and penetrate the implanted material by creating a sufficient gap [62]. However, the degradation rate of implanted materials should not be excessively fast since it should ideally match the bone osteogenic rate [63,64]. Uchida et al. [65] employed HAp as a bone implant to repair the bone after tumour excision in 60 patients at various bone sites. They observed HAp efficiently merged with host bones, and HAp implants included osteoblast cells. Even after 5 years, no symptoms of degradation were found [65]. The manufactured freeze-dried scaffold findings indicate that increasing the Fe-DCPD concentration reduces the scaffold's mass loss. The freeze-dried CH scaffold lost the most mass (39.5 ± 1.3%), whereas the 50-Fe^{3+}-DCPD scaffold lost the least (20.5 ± 1.8%) after 4 weeks. The XRD analysis demonstrates that the mass loss differential is likely owing to the 50- Fe^{3+}-DCPD's greater crystallinity than the other scaffolds. It is necessary for potential bone scaffolds and scaffold degradation products to be biocompatible to ensure that, after implantation in vivo, no cytotoxicity or inflammatory reaction would occur [66]. The freeze-dried scaffolds' cytotoxicity was assessed using direct and indirect cytotoxicity by XTT assay. The manufactured scaffolds demonstrated no harmful effects. Furthermore, indirect cytotoxicity data from the XTT experiment showed that increasing Fe^{3+}-DCPD concentration improves the percentage of cells alive in the scaffold extract.

To facilitate bone tissue regeneration or repair and the restoration of normal biomechanical performance, it is also necessary for the scaffolds used in bone tissue engineering to offer temporary mechanical strength at the site of the defect [67]. Chitosan is an excellent natural polymer to use in bone tissue engineering scaffolds. It is antimicrobial, biocompatible, and biodegradable, aiding wound healing. However, chitosan lacks the strong mechanical properties required for load-bearing applications [68]. The combination of Cs and CaP improves scaffold mechanical qualities; however, CaP does not have strong mechanical properties. Fe^{3+}-ions were shown to increase the presence of a protein required for cell adhesion in DCPD samples compared to undoped samples [69]. Fe ions in DCPD could encourage cell growth [70]. Iron is an element that occurs naturally in the human body; therefore, incorporating it into the scaffold provides no danger of toxicity or rejection. Fe^{3+} is essential for blood haemoglobin, which transports oxygen [71]. The Fe^{3+} doping of CaP enhances toughness and durability, promotes bone formation, accelerates healing, and reduces problems [69]. Thus, adding Fe^{3+}-DCPD minerals to Cs enhanced freeze-dried scaffolds' mechanical characteristics and osteoconduction. Compared to the Fe^{3+}-DCPD mineral-free CH scaffold, the overall strength of the produced scaffolds grew with increasing Fe-DCPD mineral concentration, with the 50- Fe^{3+}-DCPD scaffold demonstrating a 25.9 ± 0.19 kNm^{-2} increase in Young's Modulus and a 25.5 ± 0.13 kPa increase in tensile strength. Furthermore, it was found that Fe^{3+}-DCPD mineral-doped chitosan scaffolds had higher mechanical characteristics than DCPD mineral-doped chitosan scaffolds [72].

Strong cationic or anionic particles indicate particle stability and dispersion in solution [73,74]. All examined freeze-dried scaffolds had positive charge (+ve) zeta potentials ranging from +21 to +49 mV. The positive charge in mineral-free CH is produced from free amine groups in chitosan protonated in aqueous solutions. The mineral-free CH scaffold had the highest positive zeta potential (+48.6 ± 0.4). Adding Fe^{3+}-DCPD mineral to chitosan lowered the zeta

potential because phosphate ions have an affinity for protonated amine [75], resulting in a reduction in the particles' positive charge. Because the increase in Fe^{3+}-DCPD phosphate ions coincides with a reduction in the zeta potential.

5. Conclusions

The results of Raman, FTIR, XRD, and SEM characterisations confirm that it was possible to fabricate porous freeze-dried CH scaffolds incorporated with different concentrations of Fe^{3+}-DCPD minerals (0, 20, 30, 40, and 50 (wt) %). The crystallinity of the scaffolds increased as the Fe^{3+}-DCPD mineral concentration increased from 0 to 50 (wt) %, resulting in stiffer structures and reduced degradation and swelling rate which was tested at 37°C. The mechanical characteristics were enhanced by the addition of Fe^{3+}-DCPD minerals; 50-Fe^{3+}-DCPD scaffolds demonstrated more than five times (31.3 ± 0.06 kN) the mechanical strength of the Fe^{3+}-DCPD mineral-free scaffolds (CH, 5.4 ± 0.19 kN).

It was established swelling ratio (as shown in Figure 7) of scaffolds was larger in the first 30 minutes, which progressively reduced as the time elapsed from hours to weeks of testing each composition. The swelling ratio was found to increase with the magnitude of mass lost from the scaffolds.

The swelling and degradation of scaffolds were found to be interrelated. With an increasing volume fraction of crystalline mineral phase present in the scaffold, the swelling ratio and degradation rate reduced, which are attributed to the structural effect dependent on the interaction of the protonated surface in CS with the negative charge on colloidal Fe^{3+}-DCPD, which were confirmed in the Zeta potential measurements in Table 2.

The SEM results showed that the volume fractions of Fe^{3+}-DCPD minerals reduced the overall pore volumes and interconnected porosity in the CS-Fe^{3+}-DCPD materials, which is why the mechanical strength of the Fe^{3+}-DCPD scaffolds increased with increasing weight % of minerals, as shown in Table 3.

On days 3, 7, and 14, increasing the Fe^{3+}-DCPD concentration led to higher MSC proliferation in the 20, 30, and 40- Fe^{3+}-DCPD scaffolds. However, MSC proliferation was reduced on days 3, 7, and 14 for the 50- Fe^{3+}-DCPD scaffolds when compared to the 40- Fe^{3+}-DCPD scaffold. In summary, the addition of Fe^{3+}-DCPD minerals into chitosan improved the biocompatibility, mechanical characteristics, and percentage (%) cell viability of the scaffolds.

Author Contributions: LY synthesised, characterised, wrote and tested the freeze-dried scaffolds. AJ and PVG supervised the PhD research project in the respective areas of expertise in materials engineering and characterisation of bone biology and orthopaedic implants. NI, AJ, and PVG proofread the manuscript. All authors have read and agreed to the published version of the manuscript.

Funding: The authors acknowledge the scholarship from the Turkish Ministry of National Education, Republic of Turkiye (L Yildizbakan), Biomedical Research Centre Funding (NiHR-20331) for NI, EP/EP/K020234/1 and MRC-CiC institutional funding at the University of Leeds.

References

[1] H. Bezstarosti, W.J. Metsemakers, E.M.M. van Lieshout, L.W. Voskamp, K. Kortram, M.A. McNally, L.C. Marais, M.H.J. Verhofstad, Arch. Orthop. Trauma Surg. 141 (2021) 1215–1230.

[2] D.P. Martin, R. B., Burr, D. B., Sharkey, N. A., & Fyhrie, Skeletal Tissue Mechanics, Springer, New York, NY, 1998.

[3] W. Wang, K.W.K. Yeung, Bioact. Mater. 2 (2017) 224–247.

[4] S.T. Kao, D.D. Scott, Oral Maxillofac. Surg. Clin. North Am. 19 (2007) 513–521.

[5] B. Zárate-Kalfópulos, A. Reyes-Sánchez, Cir. Cir. 74 (2006) 217–222.

[6] J.R. Jones, L.L. Hench, Mater. Sci. Technol. 17 (2001) 891–900.

[7] M. Frohlich, W. Grayson, L. Wan, D. Marolt, M. Drobnic, G. Vunjak- Novakovic, Curr. Stem Cell Res. Ther. 3 (2008) 254–264.

[8] A. Nather, Bone Grafts Bone Substitutes Basic Sci. Clin. Appl. (2005) 1–593.

[9] P. Chocholata, V. Kulda, V. Babuska, Materials (Basel). 12 (2019).

[10] M. Rinaudo, Prog. Polym. Sci. 31 (2006) 603–632.

[11] K. Tomihata, Y. Ikada, Biomaterials 18 (1997) 567–575.

[12] M. Shin, H. Yoshimoto, J.P. Vacanti, Tissue Eng. 10 (2004) 33–41.

[13] A.S. Badami, M.R. Kreke, M.S. Thompson, J.S. Riffle, A.S. Goldstein, Biomaterials 27 (2006) 596–606.

[14] I. V. Fadeeva, S.M. Barinov, A.Y. Fedotov, V.S. Komlev, Dokl. Chem. 441 (2011) 387–390.

[15] R. Pallela, J. Venkatesan, V.R. Janapala, S.K. Kim, J. Biomed. Mater. Res. - Part A 100 A (2012) 486–495.

[16] Y. Wang, L. Zhang, M. Hu, H. Liu, W. Wen, H. Xiao, Y. Niu, J. Biomed. Mater. Res. - Part A 86 (2008) 244–252.

[17] S.M. Best, A.E. Porter, E.S. Thian, J. Huang, J. Eur. Ceram. Soc. 28 (2008) 1319–1327.

[18] C.C. Ribeiro, C.C. Barrias, M.A. Barbosa, J. Mater. Sci. Mater. Med. 17 (2006) 455–463.

[19] M. Schicker, H. Seitz, I. Drosse, S. Seitz, W. Mutschler, Eur. J. Trauma 32 (2006) 114–124.

[20] A. Laskus, J. Kolmas, Int. J. Mol. Sci. 18 (2017) 1–22.

[21] F. Barrère, C.A. Van Blitterswijk, 1 (2006) 317–332.

[22] S. V. Dorozhkin, Biomatter 1 (2011) 121–164.

[23] A. Bigi, E. Boanini, J. Funct. Biomater. 9 (2018).

[24] J. Engstrand, C. Persson, H. Engqvist, J. Mech. Behav. Biomed. Mater. 29 (2014) 81–90.

[25] P.S. Eggli, W. Muller, R.K. Schenk, Clin. Orthop. Relat. Res. (1988) 127–138.

[26] E. Alsubhe, A.D. Anastasiou, M. Mehrabi, E.M. Raif, A. Hassanpour, P. Giannoudis, A. Jha, Mater. Sci. Eng. C 115 (2020) 111053.

[27] S.B. Gary A. Fielding, Amit Bandyopadhyay, Dent Mater 28 (2012) 113–122.

[28] A. Bandyopadhyay, S. Bernard, W. Xue, S. Böse, J. Am. Ceram. Soc. 89 (2006) 2675–2688.

[29] C. Rey, O. Marsan, C. Combes, C. Drouet, D. Grossin, S. Sarda, 8 (2014) 229–266.

[30] M.M. Maskanati M, Motiee F, Aghabozorgb H, 12 (2021) 535–542.

[31] M.F. Queiroz, K.R.T. Melo, D.A. Sabry, G.L. Sassaki, H.A.O. Rocha, Mar. Drugs 13

(2015) 141–158.
[32] R. Singh, P.D. Lee, R.J. Dashwood, T.C. Lindley, Mater. Technol. 25 (2010) 127–136.
[33] S. Mandel, A.C. Tas, Mater. Sci. Eng. C 30 (2010) 245–254.
[34] S.R. Vasant, M.J. Joshi, Mod. Phys. Lett. B 25 (2011) 53–62.
[35] A.B. Vino, P. Ramasamy, V. Shanmugam, A. Shanmugam, M. Biology, Asian Pac. J. Trop. Biomed. (2012) 334–341.
[36] C. Song, H. Yu, M. Zhang, Y. Yang, G. Zhang, Int. J. Biol. Macromol. 60 (2013) 347–354.
[37] M.J.L. Dantas, B.F.F. Santos, A.A. Tavarez, M.A. Maciel, B.M. Lucena, M.V. Fook, S.M. Silva, Molecules 24 (2019) 1–20.
[38] L. Gritsch, M. Maqbool, V. Mouriño, F.E. Ciraldo, M. Cresswell, P.R. Jackson, C. Lovell, A.R. Boccaccini, J. Mater. Chem. B 7 (2019) 6109–6124.
[39] M.I. Limited, Zetasizer Nano Serles Tech. Note. MRK654-01 2 (2011) 1–6.
[40] Z. Li, H.R. Ramay, K.D. Hauch, D. Xiao, M. Zhang, Biomaterials 26 (2005) 3919–3928.
[41] X.D. Ren, Q.S. Liu, H. Feng, X.Y. Yin, Appl. Mech. Mater. 665 (2014) 367–370.
[42] S. Singh, V. Singh, S. Aggarwal, U.K. Mandal, Chem. Pap. 64 (2010) 491–498.
[43] C.M. Murphy, M.G. Haugh, F.J. O'Brien, Biomaterials 31 (2010) 461–466.
[44] G. Jia, H. Huang, J. Niu, C. Chen, J. Weng, F. Yu, D. Wang, B. Kang, T. Wang, G. Yuan, H. Zeng, J. Magnes. Alloy. 9 (2021) 1954–1966.
[45] J. Yu, H. Xia, Q.Q. Ni, J. Mater. Sci. 53 (2018) 4734–4744.
[46] S.J. Lee, I.W. Lee, Y.M. Lee, H.B. Lee, G. Khang, J. Biomater. Sci. Polym. Ed. 15 (2004) 1003–1017.
[47] L.L. Reys, S.S. Silva, J.M. Oliveira, S.G. Caridade, J.F. Mano, T.H. Silva, R.L. Reis, Biomed. Mater. 8 (2013).
[48] J.M. Oliveira, M.T. Rodrigues, S.S. Silva, P.B. Malafaya, M.E. Gomes, C.A. Viegas, I.R. Dias, J.T. Azevedo, J.F. Mano, R.L. Reis, Biomaterials 27 (2006) 6123–6137.
[49] B.S. J. J. Klawitter, J.G Bagwell, AM Weinstein, 10 (1976) 311–323.
[50] L.L. Reys, S.S. Silva, R.P. Pirraco, A.P. Marques, J.F. Mano, T.H. Silva, R.L. Reis, Eur. Polym. J. 95 (2017) 232–240.
[51] A. Kramschuster, L.S. Turng, Fabrication of Tissue Engineering Scaffolds, Elsevier, 2013.
[52] V. Karageorgiou, D. Kaplan, Biomaterials 26 (2005) 5474–5491.
[53] J.L. Paris, N. Lafuente-Gómez, M.V. Cabañas, J. Román, J. Peña, M. Vallet-Regí, Acta Biomater. 86 (2019) 441–449.
[54] S. V. Madihally, H.W.T. Matthew, Biomaterials 20 (1999) 1133–1142.
[55] C. Ji, N. Annabi, A. Khademhosseini, F. Dehghani, Acta Biomater. 7 (2011) 1653–1664.
[56] S.K.L. Levengood, M. Zhang, J. Mater. Chem. B 2 (2014) 3161–3184.
[57] M.S.B. Reddy, D. Ponnamma, R. Choudhary, K.K. Sadasivuni, Polymers (Basel). 13 (2021).
[58] E. Cohen, E. Poverenov, Chem. - A Eur. J. 28 (2022).
[59] E. Budianto, A. Amalia, J. Polym. Eng. 40 (2020) 551–560.
[60] L. Tao, L. Zhonglong, X. Ming, Y. Zezheng, L. Zhiyuan, Z. Xiaojun, W. Jinwu, RSC Adv. 7 (2017) 54100–54110.

[61] F. Ahmadi, Z. Oveisi, M. Samani, Z. Amoozgar, Res. Pharm. Sci. 10 (2015) 1–16.

[62] Z. Sheikh, M.N. Abdallah, A.A. Hanafi, S. Misbahuddin, H. Rashid, M. Glogauer, Materials (Basel). 8 (2015) 7913–7925.

[63] K. Rezwan, Q.Z. Chen, J.J. Blaker, A.R. Boccaccini, Biomaterials 27 (2006) 3413–3431.

[64] C.X.F.L. Dietmar Werner Hutmacher, Jan Thorsten Schantz, T.C. Lim, Kim Cheng Tan, J. Tissue Eng. Regen. Med. (2007) 245–260.

[65] A. Uchida, N. Araki, Y. Shinto, H. Yoshikawa, E. Kurisaki, K. Ono, J. Bone Jt. Surg. - Ser. B 72 (1990) 298–302.

[66] M.I. Echeverria Molina, K.G. Malollari, K. Komvopoulos, Front. Bioeng. Biotechnol. 9 (2021) 1–29.

[67] A.R. Amini, C.T. Laurencin, S.P. Nukavarapu, Crit. Rev. Biomed. Eng. 40 (2012) 363–408.

[68] X.-S.G.& X.-L.M. Shuai Wei, Jian-Xiong Ma, Lai Xu, Mil. Med. Res. (2020) 457–470.

[69] Y. Ikada, J. R. Soc. Interface 3 (2006) 589–601.

[70] Q. Wang, B. Chen, M. Cao, J. Sun, H. Wu, P. Zhao, J. Xing, Y. Yang, X. Zhang, M. Ji, N. Gu, Biomaterials 86 (2016) 11–20.

[71] N. Abbaspour, R. Hurrell, R. Kelishadi, J. Res. Med. Sci. 19 (2014) 3–11.

[72] N. Iqbal, T.M. Braxton, A. Anastasiou, E.M. Raif, C.K.Y. Chung, S. Kumar, P. V. Giannoudis, A. Jha, Materials (Basel). 15 (2022).

[73] J.D. Clogston, A.K. Patri, Methods Mol. Biol. 697 (2011) 63–70.

[74] B. Salopek, D. Krasic, S. Filipovic, Rud. Zb. 4 (1992) 147–151.

[75] C. De Stefano, A. Gianguzza, D. Piazzese, S. Sammartano, Chem. Speciat. Bioavailab. 22 (2010) 99–107.

Synthesis and Engineering of Cancellous Bone Scaffold Derived from Freeze-Dried Ferric-ion (Fe3+)-doped Brushite

ORIGINALITY REPORT

35%
SIMILARITY INDEX

MATCHED SOURCE

1	www.mdpi.com Internet	1597 words — 18%
★	www.mdpi.com Internet	18%

EXCLUDE QUOTES	ON	EXCLUDE SOURCES	OFF
EXCLUDE BIBLIOGRAPHY	ON	EXCLUDE MATCHES	OFF